



## HYDRAULIC BEHAVIOR OF A FRANCIS TURBINE WITH ASYMMETRICAL GUIDE VANES

**Daniel Freitas Coelho**

**Danilo de Souza Braga**

Universidade Federal do Pará, Grupo de Vibrações e Acústica. Rua Augusto Corrêa, 01 - Guamá. Belém - Pará – Brasil  
danilo.braga@itec.ufpa.br  
daniel.coelho@itec.ufpa.br

**Newton Sure Soeiro**

Universidade Federal do Pará, Grupo de Vibrações e Acústica. Rua Augusto Corrêa, 01 - Guamá. Belém - Pará – Brasil  
nsоеiro@ufpa.br

**Gustavo da Silva Vieira de Melo**

Universidade Federal do Pará, Grupo de Vibrações e Acústica. Rua Augusto Corrêa, 01 - Guamá. Belém - Pará – Brasil  
gmelo@ufpa.br

**Sergio Custódio de Souza Filho**

Universidade Federal do Pará, Grupo de Vibrações e Acústica. Rua Augusto Corrêa, 01 - Guamá. Belém - Pará – Brasil  
engsergiocustodio@gmail.com

**Abstract.** *Guide vanes are the entities that allow variation of the discharge penetrating runner, so as to attend electric power demanded. Guide vanes are actuated by servos controlled by automatic speed regulators and link the discharge with the required power. Nevertheless, the maintenance of these servos is not constant in most cases, and the guide vanes could possibly move away from the operation condition angle. This paper provides an approach of a three-dimensional unsteady turbulent flow in the entire flow passage of a Francis turbine model of a hydro power plant using finite volume method (FVM) by adopting the shear stress transport (SST) turbulence model. Using experimental data from manometers positioned on the inlet of the spiral casing, outlet of the runner and outlet of the draft tube, the mathematical model is verified. Pressure pulsations are calculated for a turbine on normal condition of operation and attached with an asymmetrical distribution of guide vanes. Hydraulic flow phenomena in the Francis turbine are analyzed and compared for both cases.*

**Keywords:** *Asymmetrical guide vanes, Francis turbine, pressure pulsations, finite volume method.*

### 1. INTRODUCTION

Many dynamic problems occurring in hydraulic machines can only be properly understood if their interaction with the fluid column in the waterways of the plant is taken into account. Non-steady pressure and flow propagate into the fluid column in the penstock and other connected pipes. Even in plants with shorter and simpler water conduits, there is always some kind of response of the water conduit to excitations from the hydraulic machine. The action of hydraulic forces generates vibrations on the runner and on the shaft which are transmitted to the bearings.

The hydraulic interaction between runner blades and guide vanes is a well-known cause of vibration and noise in all kinds of turbines. Thus, the rotor stator interaction phenomenon may be considered as a combination of inviscid flow, potential, and viscous flow, wake, interactions (Xiao *et al*, 2012). Some authors consider the application of misaligned guide vanes (MGV) for pump storage turbine brought up a new hydrodynamic research topic, including the new rotor stator interaction between the MGV and runner.

Shao (2009) proved that MGVs can improve stability of the reversible pump turbines in no-load mode and, on turbine startup mode and cut down the surge pressure rises under turbine load-rejections. In order to achieve expand applications of MGVs in high-head pumped storage plants, the internal characteristics of the reversible pump turbine with MGVs in turbine modes and reverse pump modes, the empirical formulae at runaway and zero-flow special condition point were proposed. Also, Xiao *et al* (2012) verified that MGV can decrease the peak-to-peak amplitude of pressure fluctuation in the whole flow passage except on rotating runner blades. The low frequencies and the influence of Rotor Stator Interaction (RSI) in the entire flow passage vary with the arrangement/openings of MGV. Those characteristics were used to optimize the model of MGV for pump-turbine by Sun *et al* (2012) and Liu *et al* (2012).

Currently, Computational Fluid Dynamics (CFD) is intensively used on hydraulic turbine design and research process. Steady flow analysis has been applied to successfully predict flow characteristics and energy losses in different hydraulic turbine components and used to validate experimental results. According Xiao and Yu (2010), Navier-Stokes flow simulations are commonly used on the design and optimization process of the hydraulic turbine components. To solve the equations for the problems, turbulence models are applied to study flow characteristics. Geberkiden (2007)

made comparisons between experimental data and numerical simulations using standard k- $\epsilon$  and SST k- $\omega$  turbulence models. The SST turbulent model seems to show better acceptance with the experimental results.

Different problems in hydraulic turbine arise from unsteady flow phenomena. In order to get information on this phenomena or solutions to the problems, an unsteady flow analysis is necessary. Pressure fluctuation can give more information about the system stability and must be analyzed on time and frequency domains.

Therefore, a three-dimensional unsteady turbulent flow in the entire flow passage of a Francis turbine model using FVM by adopting shear stress transport (SST) turbulence model was created. Experimental data from manometers were used for validation. After, pressure pulsations were calculated for a turbine model on normal conditions of operation and attached with different asymmetrical distribution of guide vanes to check pressure stabilization. Hydraulic flow phenomena in the Francis turbine are analyzed and compared for both cases.

## 2. MATHEMATICAL MODEL AND COMPUTATIONAL DETAILS

Since there are commonly strong interactions between guide vanes, runner and draft tube, it is inevitable to introduce these components interaction into simulations for accurate results. Following it will be briefly shown the mathematical model used computationally by finite volume method.

### 2.1 Governing equations of fluid dynamics

The governing equations for the CFD calculations are integrated over each control volume, such that relevant quantities (mass, momentum, energy etc.) are conserved in a discrete sense for each control volume. First, the equation of continuity (conservation of mass) for a general compressible fluid is expressed by:

$$\frac{\partial \rho}{\partial t} + \nabla \cdot (\rho \mathbf{U}) = 0 \quad (1)$$

Where  $\rho$  denotes the density and  $\mathbf{U}$  is the fluid velocity. For incompressible fluid  $\nabla \cdot \mathbf{U} = 0$  even if it is unsteady. Second, there is the equation of motion which prescribes the conservation of momentum:

$$\frac{\partial(\rho \mathbf{U})}{\partial t} + (\rho \mathbf{U}) \nabla \cdot \mathbf{U} = \nabla \cdot (-P \delta) + \nabla \cdot (\mu (\nabla \mathbf{U} + (\nabla \mathbf{U})^T)) + S_M \quad (2)$$

Where  $P$  is the static pressure,  $\mu$  is the dynamic viscosity and  $S_M$  is the momentum source. To Geberkiden (2007) the momentum source represents the body forces that act on the fluid particle, which are gravitational, centrifugal, Coriolis (a result of centripetal force on a mass moving with a velocity radially outward in a rotating plane) and electromagnetic forces.

The finite volume method is one of the numerical methods used in the simulation of fluid flows, especially for complex geometries. The basic characteristic that makes it suitable for this type of applications is that it is fully conservative. This means that at any mesh density level, transported quantities are fully conserved. This basic property is because the methods discretize an integral form of the governing equation, yielding a semi-discrete balance equation

$$\int_A n \rho \phi U dA = \int_A n \cdot \Gamma \cdot \text{grad} \phi dA + \int_A S_\phi dV \quad (3)$$

Where,  $\Gamma$  is the diffusion coefficient and is the source term.

### 2.2 Turbulence model

Turbulence model is defined as a set of equations (algebraic or differential) which determines the turbulent transport terms in the mean flow equation. Turbulence models are based on hypotheses about turbulent processes and require empirical input in the form of constants or functions.

The turbulence is taken into account with a two-equation model, the standard shear stress transport (SST). The mean reason to choose this model is because the results obtained seems to be more suitable with experimental data than other turbulence models. Other advantages of the SST model used on simulation are:

- To enjoy the advantages of k -  $\omega$  and k -  $\epsilon$  models by combining them.
- To make certain proper relation between turbulent kinetic energy and turbulent stress.
- To offers accurate and robust prediction of problems with flow separation.
- Strongly recommended to flow near to wall or ducts.

- Highly accurate predictions of the onset and the amount of flow separation under adverse pressure gradients.

Studies about models comparison are discussed with more details on Geberkiden (2007) and Maruzewski (2010). According the numerical studies developed by Wilcox (1986), the two partial differential equations governing the turbulent kinetic energy  $k$  and the turbulent frequency  $\omega$  then reads:

$$\frac{\partial(\rho k)}{\partial t} = P_k - D_k + \nabla((\mu + \sigma_k \mu_t) \nabla k) \quad (4)$$

$$\frac{\partial(\rho \omega)}{\partial t} = \alpha \rho \frac{P_\Omega}{\mu_t} - D_\omega + C d_\omega + \nabla((\mu + \sigma_k \mu_t) \nabla \omega) \quad (5)$$

where  $P_k$  and  $P_\Omega$  are production terms,  $D_k$  and  $D_\omega$  destruction ones and  $C d_\omega$  results from transforming the  $\varepsilon$  equation into an equation for  $\omega$ . The coefficients in the SST model are obtained by combining the value of the coefficients of the standard  $k - \omega$  (in the near wall region) to those of the  $k - \varepsilon$  model by using a blending function  $F_1$ . Studies about coefficients are discussed with more details on work of Wilcox (1986).

### 2.3 Pressure pulsation

Experimental results proposed by Egusquiza *et al* (2012) show that the pressure pulsation generated by the RSI shows an almost regular sine-wave signal. From the rotating reference frame, any blade of the runner receives  $Z_v$  pressure pulsations for each runner revolution. Thus, its frequency is:

$$f_p = n z_v \cdot f_n \quad (6)$$

where  $f_p$  is the pressure fluctuation frequency on the runner,  $z_v$  is the number of guide vanes and  $f_n$  is the shaft rotating frequency. According to the authors, each blade receives the same pressure pulsation but with a phase shift. The amplitude of the pressure fluctuation depends on the head, the operating conditions and the design. It was measured using a pressure transducer located in the guide vane channel.

The shape of the pressure pulsation generated by the RSI around the whole runner can be determined by the following equation:

$$m z_g \pm k = n z_b \quad (7)$$

where  $n$  and  $m$  are integers,  $z_g$  is the number of guide vanes,  $z_b$  is the number of runner blades, and  $k$  is the diametrical mode.

## 3. COMPUTATIONAL MODEL

### 3.1 Characteristics of the turbine

A turbine is chosen to meet certain values of head and discharge, in which depends of the power plant conditions where it is installed. This choice also depends of another magnitude, which is the number of rotations per minute of the electric generator the turbine will operate (Macintyre, 1983).

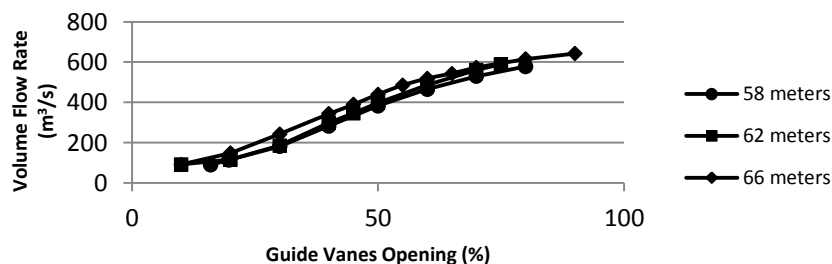


Figure 1. Mass flow rate varying with guide vanes opening and water head.

The hydro generator chosen for the analysis has on its runner 12 blades, its diameter of reference is 8.185 meters. There are 24 guide vanes and stay vanes including the spiral casing tongue. The runner nominal rotation is 81.82 rpm

and the specific speed of the turbine is 295.4 rpm in a mean water head of 60 meters giving a power of 360 MW. Fig. 1 shows the mass flow rate of the turbine varying with the guide vanes opening and water head.

**3.2 Francis turbine modeling**

The first step is building the geometrical model of the structural components of the turbine: spiral casing, guide vanes, stay vanes, runner and draft tube, according to the building documents provided. Later, there must be represented the fluid domain included on the facilities of the hydro generator, splitting the fluid domain in 3 domains: one rotating domain and two stationary domains (see Fig. 2). For the computational model it was used a 50% opening of the guide vanes, which is the most critical situation of a hydro generator according to Brandão (1987).

There was induced misalignment of 20° on some guide vanes, creating 4 models, with one MGV in each case. The location of the MGV is showed on Fig. 3 for all four cases.

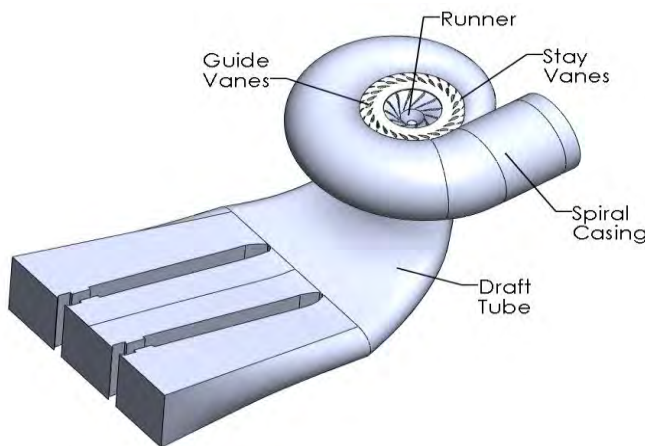


Figure 2. Fluid domain for the computational model.

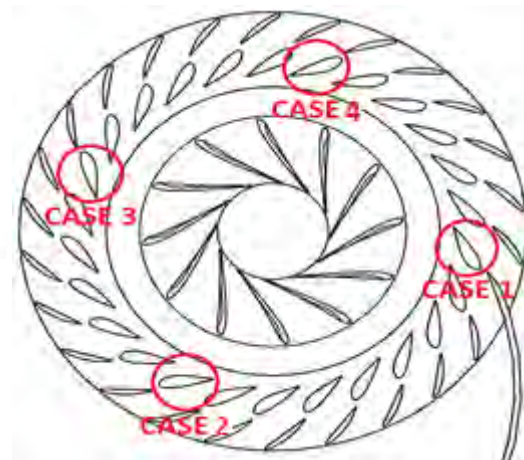


Figure 3. Location of MGV for each case.

**3.3 Mesh generation**

The fluid domain discretization can be accomplished by multiple means, but the most often adopted in three-dimensional CFD are based on either tetrahedral or hexahedral volumes. A mesh that consists of mainly tetrahedral elements is referred to as unstructured mesh while a structured mesh is comprised of hexahedral elements. For the computational domain, unstructured 3D tetrahedral meshing has been employed, due to its flexibility when solving complex geometries.

It was introduced for the principal regions of interest a concept of mesh of inflation. It creates a growing mesh which provides an acceptable prediction of the boundary layer outside the wall. There was made a mesh convergence of the model, picking 5 points and measuring pressure or velocity varying with the number of elements of the mesh. The normalized pressure or velocity varying with the number of elements for a steady solution is showed on Fig. 4. Figures 5 and 6 show the comparison between a mesh with 7.254E6 and 41.038E6 elements for pressure on runner blades and velocity around guide vanes and stay vanes.

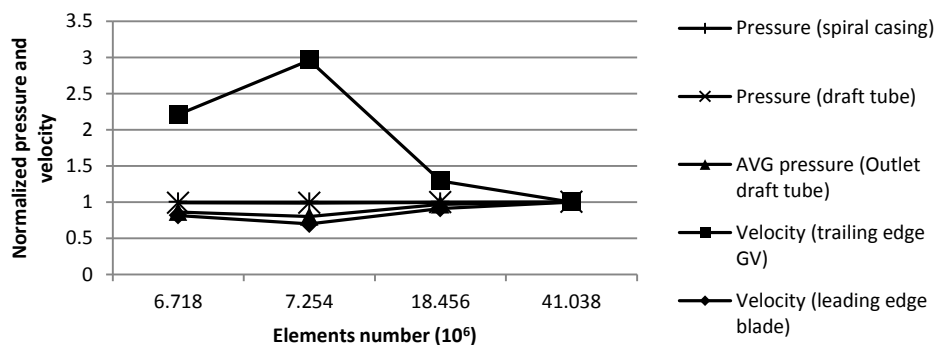


Figure 4. Normalized pressure or velocity on 5 points of the model varying with elements number.

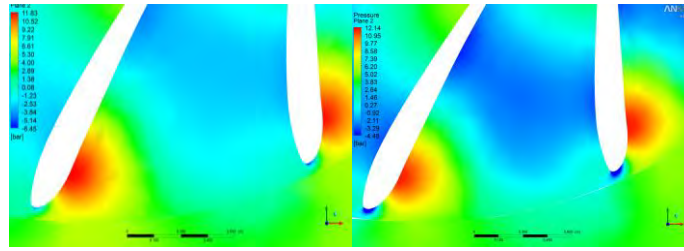


Figure 5. Contours of pressure of runner blades on middle plane of spiral casing.

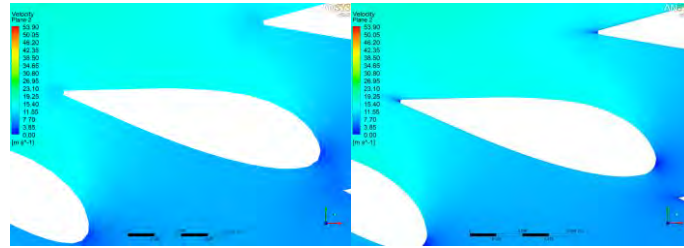


Figure 6. Contours of velocity of guide vanes and stay vanes on middle plane of spiral casing.

### 3.4 Calibration of the computational model

The present study on this section includes the calibration performed from experimental-operational testing, which was used sensors (piezometric pipe installed in the machine) distributed on turbine to perform pressure measurements during operation of the turbine to the guide vanes opening on 50 percent. The pressure transducers are capacitive differential type, positioned at 6 different points and monitored for a period of 12 hours in continuous operation. Thus, the global values measured are compared with the results obtained by the numerical model in steady state.

In the turbine of the present study, there are several manometers, from which can be used to verify the accuracy of the CFD calculations. In order, there are four manometers located on the spiral casing, in which they take an average of static pressure for four points and one manometer located on the outlet of the runner (see Fig. 7). Static pressure on the outlet of the draft tube is estimated by the meters of water column downstream, calculated on Eq. 8. Some measurement points could not be used, because they do not fit on the fluid domain of the model, unfortunately. The static pressure measured on the manometers (red lines) is compared with CFD steady results (blue lines) on Fig. 8. Estimated and calculated outlet average pressure are, respectively, 2.694 bar and 2.109 bar.

$$p_{s_{outlet}} = p_{atm} + \rho gh \quad (8)$$

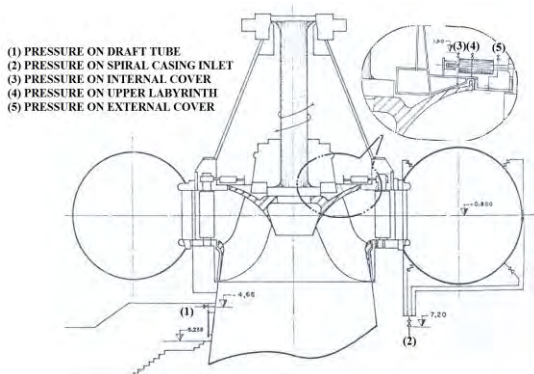


Figure 7. Manometers located on the turbine.

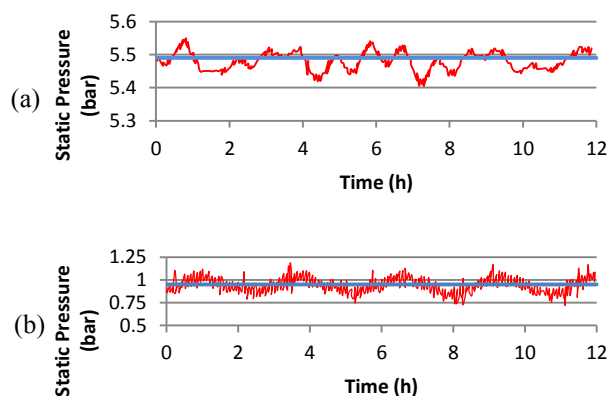


Figure 8. (a) Calibration of the measured draft tube point; (b) and spiral casing points.

### 3.5 Boundary Conditions

According to White (1991), for a fluid flow, five types of boundary conditions are considered: (i) a solid surface (can be porous), (ii) a free fluid surface, (iii) a liquid-vapor interface, (iv) a liquid-liquid interface and (v) sections of

inlet and outlet. The cases (ii) and (iii) are related because a free fluid surface is a special case of a liquid-vapor interface in which the vapor causes a negligible interaction. The only cases of boundary conditions used for the model in this paper are (i), (iv) and (v) due to the flow characteristics of the turbine.

### 3.5.1 Conditions on a solid surface

For a liquid, the molecules are so compact and the molecular distance so small, that the particles of fluid in touch to the wall must essentially be in equilibrium with the solid surface. The liquid will adhere on the wall surface (no-slip condition) and will assume the temperature of the wall. Thus, the velocity on the liquid surface equals to the velocity on the solid surface, so as the temperature.

In CFD softwares, the wall function used is an extension of the method of Launder and Spalding (1974). On the near wall regions, the tangential velocity is related to the shear stress on the wall, by a logarithmic relationship,  $u^+$ , in which is shown on Eq. 9. Where  $\kappa$  is the von Karman constant, in which for smooth walls equals to 0.41,  $y^+$  is the dimensionless distance from the wall, shown on Eq. 10, and  $C$  is a constant that depends on the roughness of the wall.

$$u^+ = \frac{1}{\kappa} \ln(y^+) + C \quad (9)$$

$$y^+ = \frac{\Delta n \sqrt{\tau_\omega / \rho}}{\nu} \quad (10)$$

Where  $\Delta n$  corresponds to the distance between the first and second node of the mesh out of the wall,  $\tau_\omega$  is the shear stress on the wall,  $\rho$  e  $\nu$  corresponds to the density and viscosity of the fluid, respectively.

The value of  $\Delta n$  can be changed according to the wall function. Three types available on ANSYS CFX are: (i) standard wall function (ii) scalable wall function e (iii) automatic wall treatment. For the first and second,  $\Delta n = \Delta n/4$  and for the third,  $\Delta n = \Delta n$ . Thus, turbulence models like  $k-\omega$  e SST in which use automatic wall treatment need a better refinement on the mesh near the walls. In the sense that, for numerical simulations that require high accuracy, like heat transfer predictions, it is recommended an  $y^+$  around 1.

### 3.5.2 Liquid-liquid interface conditions

In a real liquid-liquid interface, the superior fluid is strongly coupled and exercises kinematic, stress and energy constraints. The fluids motions are made simultaneously and must correspond in a determined way on the interface. An interface cannot store momentum or thermal energy, thus the total velocity, shear stress and temperature must be continuous through the interface.

For the numerical simulation, the interface model General Connection performs the connection between two regions that belongs to distinct fluid domains. This can be used to connect meshes that do not correlate, or apply the change of interface between rotor and stator. The GGI algorithm (General Grid Interface) is used in both cases.

For interfaces between rotor and stator it is used the Frozen Rotor model, in which the velocity field on the interior of the rotating domain is solved in relation to a rotating referential, whereas the velocity field on the external domain is solved in relation to a stationary domain. This will give a steady flow, in which no transient effect is included. Simulations with the Frozen Rotor model are performed, to obtain initial values and assign them in a transient simulation.

For transient final models, it was used a Transient Rotor-Stator interface, where the interface position is updated each timestep, as the relative position of the grids on each side of the interface changes, therefore it predicts the true transient interaction of the flow between a stator and rotor passage.

The interfaces assigned to the turbine model are shown on Fig. 9, both rotor-stator interfaces, one between runner and guide vanes (Interface 1), and other between runner and draft tube (Interface 2).

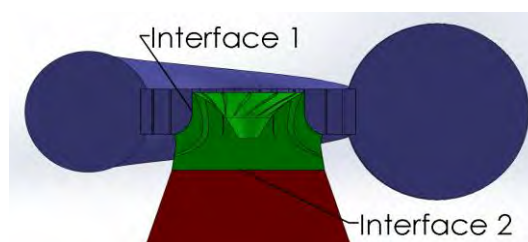


Figure 9. Interfaces between runner and guide vanes and between runner and draft tube.

### 3.5.3 Inlet and outlet conditions

It is permissible to specify the properties of the flow, on the inlet and outlet. For mathematical accuracy, would have to know the values of velocity, pressure and temperature for each point, in the planes on the inlet and outlet, however mostly this is impractical. Instead, the equations of motion are simplified, until it is less necessary the knowledge of boundary regions. For example, in an analysis of a hydraulic tube, it should be neglected the temperature variations (isothermal hypothesis) and assume that the pressure is constant through a section (one-dimensional hypothesis) (White, 1991).

For this model, the velocity profile at the inlet is assumed to be uniform and its magnitude is determined by the mean flow in the turbine data. The total pressure is specified at the inlet boundary obtained on Eq. 11, using static pressure ( $p_s$ ), and mass flow rate ( $Q$ ) from measured data. Mass flow rate is specified at the outlet boundary.

$$p_0 = p_s + \frac{\rho}{2} \left( \frac{Q}{A_{inlet}} \right)^2 \quad (11)$$

In some situations, it is suitable to specify a uniform value of the amount of turbulence on inlet regions. The turbulence can be determined by the turbulence intensity, shown on Eq. 12. Where  $u'$  is the root mean square of the velocity fluctuations,  $u_{avg}$  is the average velocity of the flow on the inlet and  $Re_{D_h}$  is the Reynolds number for a duct with  $D_h$  diameter.

$$I = \frac{u'}{u_{avg}} = 0.16 (Re_{D_h})^{-1/8} \quad (12)$$

Another parameter to determinate is the turbulence length scale ( $l$ ), which is a physical quantity describing the size of the large energy-containing eddies in a turbulent flow. An approximation between  $l$  and the physical size of the duct is defined by Eq. 13.

$$l = 0.07 D_h \quad (13)$$

#### 4. RESULTS AND DISCUSSION

To calculate the pressure pulsations, it was necessary to select points on the turbine. Xiao and Yu (2010) selected 3 points: on draft tube cone, in front of runner and at the spiral casing inlet center. For this work, the measurement points for CFD calculation were located on manometer of draft tube (green dot from Fig. 10), center of draft tube 4 meters below draft tube entrance (blue dot from Fig. 10), spiral casing entrance on mid plane (red dot from Fig. 11) and between guide vanes and runner on mid plane (pink dot from Fig. 11).

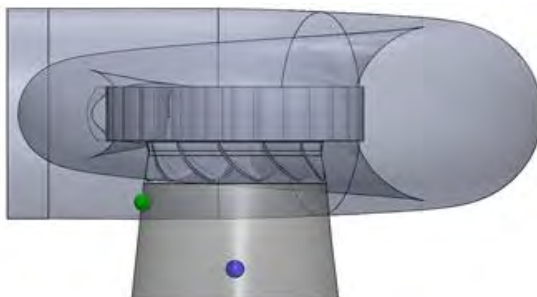


Figure 10. Points located on draft tube.

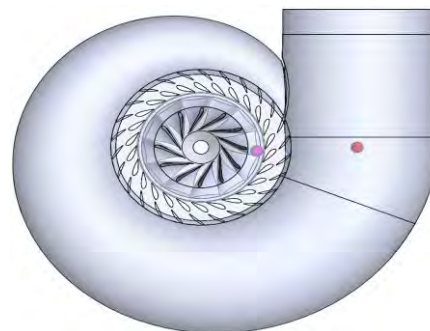


Figure 11. Points located on mid plane of spiral casing.

The total time assigned to the simulation was the time of one revolution. Since the runner rotates at 81.82 rpm, the total time for simulation was 0.7334 seconds, which was divided into 500 time steps. The computer used for calculation possesses an INTEL CORE i7 X990 3.47 GHz, 24 GB RAM, depending on 5.4E04 seconds average time of simulation for each transient case.

For the initial time, it can be seen on all cases quoted the varied behavior of vortex rope on the draft tube cone. Figure 12 shows the whirl raised for normal condition and cases 1 to 4, respectively. It is observed that the hydraulic behavior of cases 1 and 4 is similar, even as cases 2 and 3, and all reasonably differ from the normal condition (without MGv). Since it was picked 4 from 26 guide vanes to evaluate the MGv condition, it is assumed that the guide vanes on the interval between cases 1 and 2, between cases 2 and 3, and so on, is reasonably an interpolation from these results.

C. F. Daniel, B. S. Danilo and S. S. Newton  
Hydraulic Behavior of a Francis Turbine with Asymmetrical Guide Vanes

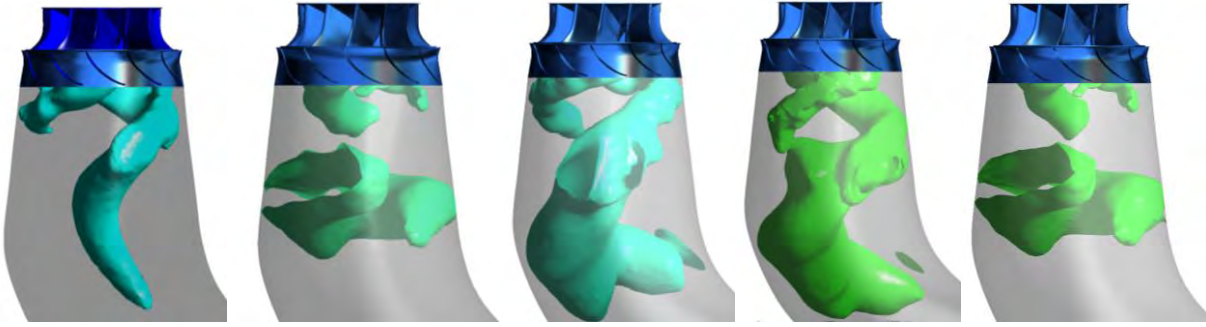


Figure 12. Vortex rope for all cases quoted.

Results on time domain for RSI point is shown on Figure 13. Both normal condition and Case 1 reveal a similar behavior, only with different magnitude for several timesteps. The sine-wave form of the curves shows an agreement with experimental results proposed by Egusquiza *et al* (2012).

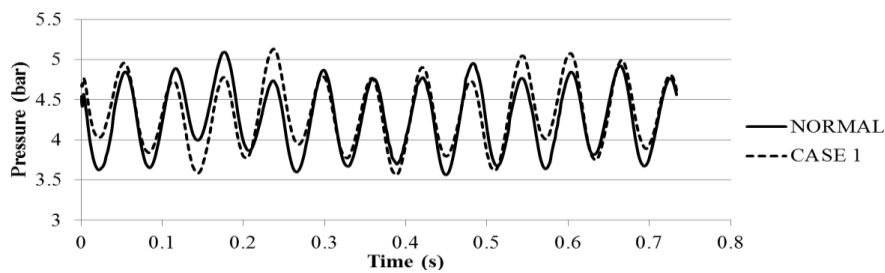


Figure 13. Pressure pulsation on RSI point for normal operation and Case 1.

The pressure fluctuation is calculated among different MGV schemes. The pressure measuring points are shown in Figure 14 to 17. The pressure pulsation in hydraulic turbine were first related to the pressure pulse on the draft tube (4 m below entrance), which are shown on Fig. 14. The water pressure pulses on draft tube entrance a dominant frequency of  $0.25f_p$  (runner rotation frequency), in concordance with results observed Xiao and Yu (2010) and Xiao *et al* (2008), which was between  $1/2$  and  $1/5 f_p$ . The dominating frequency in the draft tube cone is 4.082 Hz. Also, harmonics of rotation frequency can be observed.

Following, other point on draft tube (manometer position) showed on Figure 15, was used to compare with the point mentioned earlier, where vortex rope swirling frequency remains being the dominating frequency, however, a new characteristic MGV frequency can be observed next to 10 Hz and runner rotation frequency still appear with harmonics (16.33 and 32.66 Hz).

The low-frequency pressure pulsation can propagate upstream from the draft tube cone to the spiral casing inlet with the reduction of amplitude. The high-frequency in front of runner has the same character.

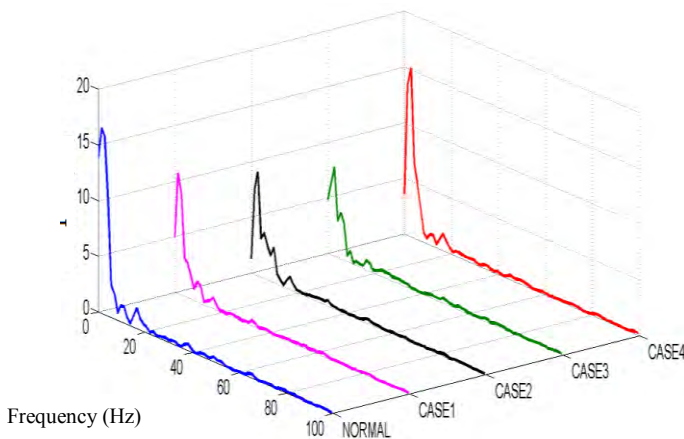


Figure 14. Frequency domain for the draft tube entrance.

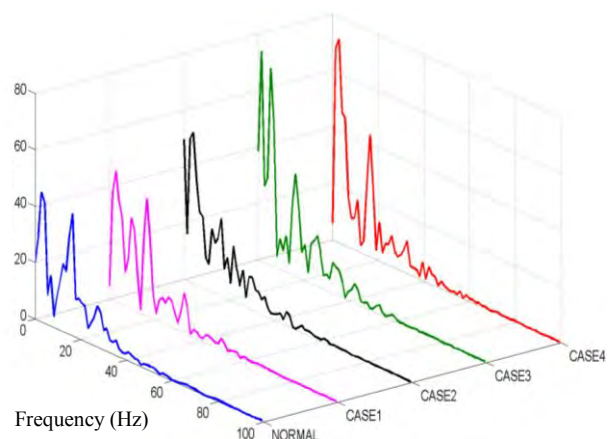


Figure 15. Frequency domain for the draft tube manometer.

The pressure pulsation spectrum in RSI gives two types of frequency, shown in Fig. 16. One is the same frequency observed on draft tube manometer point (9.526 Hz), another is the frequency of the vortex rope 4.082 Hz. The magnitude on the first mentioned frequency increases on MGV cases, mostly on Cases 2 to 4. The harmonics of runner rotating frequency can be observed.

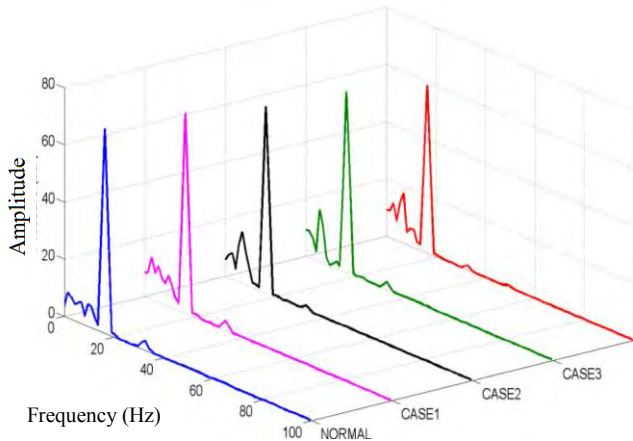


Figure 16. Frequency domain for the RSI point.

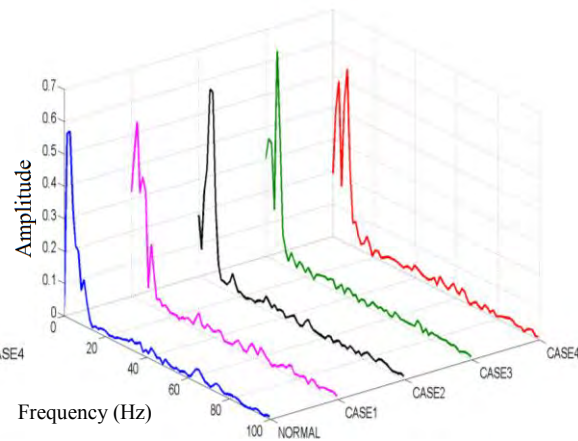


Figure 17. Frequency domain for the spiral casing entrance.

The dominating frequency at the spiral casing point on normal conditions is 4.082 Hz, which is the same as that of draft tube, shown on Fig. 8. However, other MGV frequency was observed, around 5.443 Hz. This point shows good sensibility to pressure pulsation, especially to MGV cases 1 and 4. The harmonics observed on other points were also identified on spiral casing. All pressure pulsation frequencies have very low amplitude.

## 5. CONCLUSION

With the increasing of unit power and size, a special attention has paid to the hydraulic turbine stability. In order to get solutions to the stability problem an unsteady flow analysis is necessary. But unsteady simulations have in common a quite large requirement of computational resources, especially for rotor-stator interactions. The complete turbine has to be considered and all flow channels in the stator as in the rotor have to be included. This leads to a refined mesh and an enormous computational effort (approximately 5.4E4 seconds). The pressure fluctuation in a Francis turbine was investigated numerically under the turbine operation for 4 different cases of misaligned guide vanes arrangement/openings and 4 different points. The appropriate boundary conditions were taken account in this paper to determine the flow characteristics of the turbine.

Since the flow has vortex instability as vortex rope in a draft tube and is dominated by disorderly effects, it is necessary to apply nonlinear models or Reynolds-stress models. Thus, the frequencies and amplitudes of integral quantities (e. g. forces) can be predicted with sufficient accuracy for most of the problems. Predicting flow phenomena and its potential of influence on each component of the model.

Misaligned guide vanes (MGVs) increase the instability of the turbines in operating mode. The surge pressure rises under turbine as was observed on measure points, showing characteristic frequencies on spiral casing, between runner and guide vanes and draft tube entrance. Draft tube vortex rope frequency remains around  $1/2$  and  $1/5f_r$ , as observed also by Xiao and Yu (2010) and Xiao *et al* (2008). MGV characteristics can be observed next to 10 Hz on draft tube manometer and RSI point, shown on Fig. 15 and 16. Pressure magnitude increases on MGV cases. Other MGV frequency was observed in spiral case points, around 5.443 Hz. The harmonics runner rotation frequency can be observed on all charts (16.33 and 32.66 Hz).

The results show that the proposed theories can be employed to achieve the characteristic frequencies of MGVs for the Francis turbine plants and prevent failures due excessive vibrations. In other hand, vibration analysis of hydro power plants is a difficult subject of study due to the complexity of the excitation forces, which change with the operating conditions, and due to the complexity of the structural response that is affected by fluid interaction. Nevertheless, this analysis is convenient for effective vibration diagnostics.

## 6. REFERENCES

- Brandão, J.G., 1987. *Vibrações em turbinas Francis com ênfase em vórtice de núcleo*. Master's thesis, Universidade Estadual de Campinas, Brazil.
- Egusquiza E., Valero, C., Huang, X., Jou, E., Guardo, A., Rodriguez, C., 2012. "Failure investigation of a large pump-turbine runner". In *21th Symposium on hydraulic machinery and systems – IAHR2002*. Lausanne, Switzerland.

C. F. Daniel, B. S. Danilo and S. S. Newton  
Hydraulic Behavior of a Francis Turbine with Asymmetrical Guide Vanes

- Geberkiden, B.M., 2007. *Effects of inlet boundary conditions on spiral casing simulation*. Master's thesis, Lulea University of Technology, Sweden.
- Lauder, B.E. and Spalding, D.B. "The numerical computation of turbulent flows". In *Computer Methods in Applied Mechanics and Engineering*, 3:269-289, 1974.
- Liu, D.M., Zheng, J.S., Wen, G.Z., Zhao, Y.Z. and Shi, Q.H., 2012. "Numerical simulation on the "S" characteristics and pressure fluctuation of reduced pump-turbine at start-up condition". In *26<sup>th</sup> Symposium on Hydraulic Machinery and Systems - IAHR2012*. Beijing, China.
- Macintyre, A.J, 1983. *Máquinas motrizes hidráulicas*. Guanabara Dois, Rio de Janeiro, 1983.
- Maruzewski, P., Hayashi, H., Munch, C., Yamaishi, K., Hashii, T., Mombelli, H.P., Sugow, Y. and Avellan, F., 2010. "Turbulence modeling for Francis Turbine water passages simulation". In *25<sup>th</sup> Symposium on Hydraulic Machinery and Systems - IAHR2010*. Timisoara, Romania.
- Shao, W.Y., 2009. "Improving stability by misaligned guide vanes in pumped storage plant". In *Power and Energy Engineering Conference - APPEEC2009*. Asia, Pacific.
- Sun, H., Xiao, R.F., Yang, W. and Liu, W.C., 2012. "The optimal model of misaligned guide vanes for a particular pump-turbine". In *26<sup>th</sup> Symposium on Hydraulic Machinery and Systems - IAHR2012*. Beijing, China.
- Wilcox, D.C., 1986. "Multiscale model for turbulent flows". In *24th Aerospace Sciences Meeting - AIAA1986*. Reno, Nevada.
- White, F.M. *Viscous fluid flow*. McGrawHill, 1991.
- Xiao, H. and Yu, B., 2010. "Hydraulic design of water turbine based on the Computational Fluid Dynamics". In *2010 International Conference on Electrical and Control Engineering - IEEE2010*. Wuhan, China.
- Xiao, Y.X., Sun, D.G., Wang, Z.W., Zhang, J. and Peng, G.Y., 2012. "Numerical analysis of unsteady flow behaviour and pressure pulsation in pump turbine with misaligned guide vanes". *IOP Conf. Series: Earth Environment*, Vol. 15, p. 032043.

## 7. RESPONSIBILITY NOTICE

The authors are the only responsible for the printed material included in this paper.